AIAA-2024-3634

The Evolution of Streamwise Vortices Formed by Inclined and Swept Round Jet within a Turbulent Boundary Layer

Barnabas Toth[1], Derek A. Nichols[2], Bojan Vukasinovic[3] and Ari Glezer[4]
Georgia Institute of Technology, Atlanta, GA 30332-0405

Matthew C. DeFore[5] and Chris Harris[6]
Northrop Grumman Aeronautics Systems

The interaction of a round surface jet with a flat plate turbulent boundary layer [Re_x = O(10^6)] in a uniform stream is investigated in wind tunnel experiments. The jet whose diameter *d* is an order of magnitude smaller than the local characteristic boundary layer thickness issues at a range of prescribed pitch and yaw angles relative to the free stream. Of specific interest are spanwise distributions of cross stream momentum flux relative to the baseline boundary layer and the evolution of uneven counter-rotating axial vortex pairs that are induced by the shear between the cross flow and the jet. It is shown that momentum flux increment through streamwise-normal planes 75*d* downstream of the jet's orifice relative to the baseline boundary layer decreases monotonically with yaw angle, and can even evolve into a slight momentum deficit. While the axial vortex on the starboard side of the yawed jet becomes weaker with increasing yaw angle as the leeward side vortex intensifies it nevertheless persists downstream and can be detected even at 50*d*. The dominant axial vortex intensifies (as measured by its circulation) with increasing yaw and lower pitch angles and often spawns a secondary axial vortex of opposite sense near the surface.

I. Introduction

Jets in cross flow are ubiquitous in a broad range of applications and have been studied extensively in numerous configurations over the years (e.g., Margason, 1993). The classical and most thoroughly studied example of jets in crossflow is the transverse jet, issuing normal and aligned in the direction of the cross flow whose interaction with the jet results in the formation of a pair of counter-rotating vortices along the spanwise edges of the jet. Early investigations of the flow were motivated by atmospheric mixing, but they have rapidly evolved to include flows related to species mixing, cooling, aerodynamic maneuvering, etc., as outlined in detailed review articles by Mahesh (2013), Karagozian (2014), and Sharmishtha and Utpal (2017).

Motivated by interest to utilize jets in cross flows as 'active' vortex generators in boundary layers over solid surfaces, Johnston and Nishi (1990) used surface-inclined jets for deliberate formation of streamwise vortices of prescribed sense. They produced configurations of co- and counter-rotating vortices by using inclined surface actuation jets that are yawed relative to the direction of

1 Graduate Research Assistant, AIAA Member.
2 Graduate Research Assistant, AIAA Member.
3 Research Engineer, AIAA Member.
4 Professor, AIAA Fellow.
5 Sr. Engineer, AIAA & INPSI Member.
6 Technology Development.

the cross flow and noted the effect of jet yaw on delaying separation. In a later investigation, Compton and Johnson (1992) studied the effects of yaw angle and velocity ratio of an inclined jet on the vorticity and circulation of the ensuing dominant streamwise vortex and reported that stronger vortices were formed at yaw angles between 45^o and 90^o, and at higher velocity ratios. The effect of the jet inclination (pitch) angle at fixed yaw (45^o) was studied by Zhang and Collins (1997) using a rectangular jet and they reported that at pitch angles greater than 45^o, the induced vortex pierced through the surface boundary layer (the effect of the velocity ratio was not reported). In a later review of vortex generator jets, Johnston (1999) noted that strong, single-sense vortices are formed by inclined jets at pitch angles below 45^o that are yawed within 60^o and 90^o. Bray and Gary (1999) developed parametric fit expressions that relate vortex circulation to the jet pitch and yaw, mass flow rate, and its plenum pressure. In a later study Milanovic & Zaman (2003) measured the flow downstream of highly inclined jets in a flat plate boundary layer over a range of yaw and pitch angles, jet momentum ratio and boundary layer thickness and characterized the peak streamwise vorticity noting that highly yawed jets remain closer to the surface, enhance the turbulence intensity within the boundary layer, and reach their peak vorticity farther downstream. Rixon and Johari (2003) showed that the circulation of streamwise vortices that are contained within the boundary layer increases linearly with jet velocity ratio when the vortices are overlaid. More recently, Feng et al. (2018) proposed a model that predicts the evolution of a jet in a cross flow based on its pitch and yaw angles and velocity ratio and argued that the evolution of the ensuing single-sense vortex in the far-field is an extension of the jet in that its penetration and circulation increase and decrease as 1/3 and -1/3 power of the streamwise distance, respectively.

While many aspects of the evolution of inclined yawed jets in cross flow have been investigated since the 1990s, few prior investigations considered the evolution of jets within a turbulent boundary layer having a characteristic scale that is significantly larger than the scale of the jet. The present investigations specifically consider the interactions of inclined yawed jets within a nominally 2-D cross flow over a flat plate such that the ensuing jet-induced vortical structures remain bounded within the turbulent boundary layer with specific attention to streamwise changes in momentum flux and turbulent characteristics and structure and strength of the streamwise vorticity concentrations relative to the base flow. Details of the features and the spatial evolution of the vortical structures induced by the jet cross flow interactions are investigated using stereo PIV measurements over a range of jet momentum flux and pitch and yaw angles.

II Experimental Setup and Flow Diagnostics

The present investigations are conducted in an open-return, low-speed wind tunnel (Figure 1) driven by a 150 HP blower (up to 95,000 CFM) with a 10:1 contraction downstream of a turbulence management section having a square test section measuring 106 cm on the side and 304 cm in length. The bottom wall of the test section was replaced with a horizontal flat plate model that can be translated vertically. The tunnel's test section is optically transparent from three sides to enable optical measurements using PIV and flow visualization. Prior to the installation of the flat plate model, the flow uniformity across the tunnel's test section was verified using Pitot probe measurements over a square grid at a range of crosswind speeds. The flat plate model is fabricated from a monolithic composite having a honeycomb core, sandwiched between two aluminum plates. The plate spans the full width of the tunnel's test section and is designed to be mounted so that it splits the airflow downstream of the contraction (Figure 1) to form a spanwise-uniform boundary layer over its upper surface downstream of a bullnose half cylinder leading edge. The

plate is attached on its lower surface to a light aluminum frame connected to four electric risers to enable adjustment of its elevation and streamwise inclination within the test section. Although in the present experiments the plate orientation is horizontal (zero pressure gradient), it is also possible to accommodate small favorable and adverse streamwise pressure gradients. The plate incorporates an interchangeable cylindrical jet module that forms an inclined yawed jet of diameter d relative to the cross flow (about 1,150d downstream from the plate's leading edge). In the present investigation stereo PIV measurements are acquired in the three streamwise-normal y-z planes x = 25, 50, and 75d (relative to the center of the jet) and the PIV optical setup is shown in Figure 1. The plate is also instrumented with two surface static pressure arrays along the plate's centerline and across the plate span upstream of the jet module.

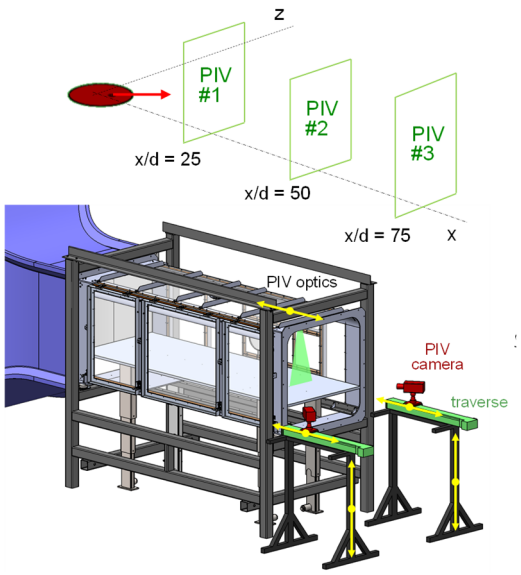

Figure 1. *CAD drawing of the wind tunnel's test section showing the moveable flat plate model and the PIV optical setup. Schematics of the experimental setup, three PIV measurement planes.*

The jet flow is formed using interchangeable cylindrical modules that are fabricated using stereolithography. Each jet module includes integrated internal contraction leading to a round conduit that forms a round jet orifice of diameter d. The 12d diameter module (Figure 2) fits within a mating opening in the plate so that its upper surface is flush with the surface of the plate. The centerline of the jet conduit of each module is inclined at a fixed pitch angle α relative to the surface such that its exit plane intersects the horizontal plate surface. In addition, the module assembly is designed to be rotated about its centerline for continuous variation of the jet's yaw angle β relative to the free stream. In the present experiments α = 20°, 32.5°, and 45° and for each of these jet modules, β was varied between 0° and 90° in equal increments of 15°. In all experiments, the origin of the coordinate systems is placed at the center of the modules (Figure 1).

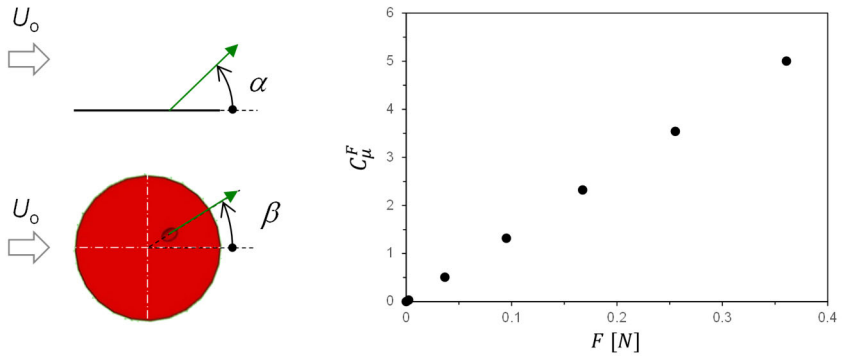

Figure 2. *Side and top views of the jet exit plane on the plate's surface showing the jet pitch and yaw angles, α and β respectively, and the jet momentum coefficient.*

In the present investigations, the jet is characterized by the ratio of the jet momentum flux to the boundary layer momentum flux (rather than by the conventional ratio of the jet momentum to the outer flow momentum). The jet momentum flux (or jet force) F is measured directly in bench tests outside of the tunnel using a 3-axis load cell over a range

of independently measured mass flow rates. The force F effected by the jet is used to define a momentum coefficient $C_\mu^F = F/(\rho \cdot U_0^2(\delta - \theta) \cdot d)$, where the denominator represents the momentum flux within the boundary layer across the jet orifice d. The coefficient C_μ^F thus serves as a measure of the aerodynamic load the jet imposes on the boundary layer of the cross flow. Figure 2 shows the jet calibration that relates the momentum ratio to the jet force F (in the present work, C_μ^F = 0.5, 2.3, and 5).

III. Interaction of the Inclined Yawed Jet with the Boundary Layer

To illustrate the effect of the jet yaw angle on its interaction with the cross flow boundary layer, the evolution of a jet having a pitch angle of $\alpha = 45°$ with yaw angles $\beta = 0°$, 30°, 60°, and 90° (i.e., pointing towards $z > 0$) is investigated using stereo PIV. It is anticipated that at this range of yaw angles the sense of the dominant streamwise vortex formed by the jet is CCW when viewed in the upstream direction. The evolution of the jet flow is depicted in a sequence of color raster plots of the time-averaged streamwise velocity overlaid with in-plane velocity vectors in the streamwise-normal plane $x = 25d$ as shown in Figure 3. The distributions of the streamwise velocity in Figures 3a-d indicate its monotonic vertical diminution towards the surface (owing to slight surface reflections these distributions do not include the surface) and spanwise changes in flow symmetry owing to the presence of the jet. When $\beta = 0°$ (Figure 3a) the jet is aligned in the streamwise direction the distribution of the in-plane velocity vectors indicates the presence of a nearly-symmetric pair of streamwise vortices that are induced about the jet's spanwise-normal center plane and are displaced above the surface by the jet pitch. It is noteworthy that the core of each vortex (as indicated by the rotational flow) exhibits a significant concentration of streamwise momentum as is evident by the two (nearly symmetric local peaks in streamwise velocity. The center of the jet in each of Figures 3a-d is marked for reference by a solid circle indicating the peak momentum in the measured flow field. It is also noted that the centers of the vortices are slightly below the peak momentum of the jet, and they induce nearly symmetric upwash of the near-surface flow underneath (the vortical composition of the flow is discussed in more detail in §IV). Several topological features of the jet change when the yaw angle is increased to $\beta = 30°$, i.e., pointing towards $z > 0$, Figure 3b). To begin with, the spanwise position of the jet's center (peak momentum) increases (its elevation increases slightly), while the plane that partitions between the two counter-rotating vortices is tilted clockwise and is accompanied by an asymmetric left to right

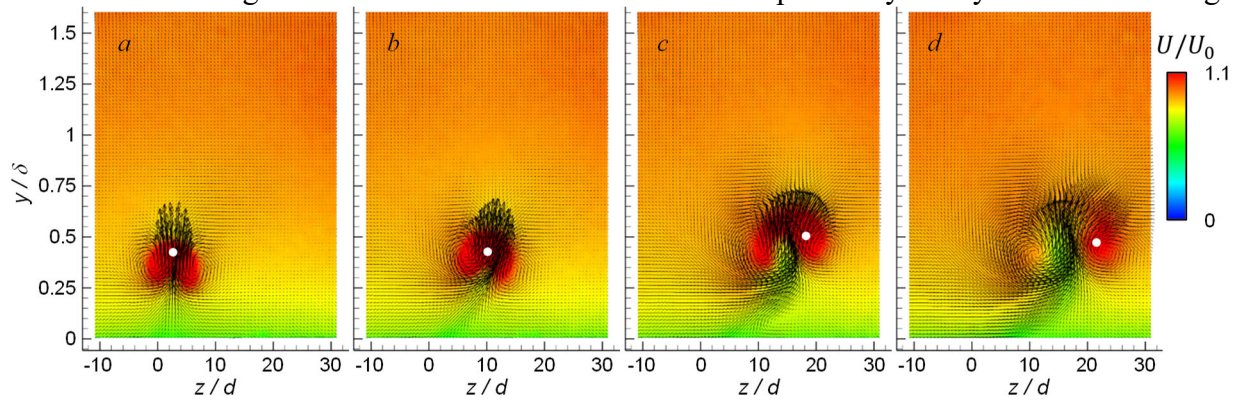

Figure 3. *Color raster plots of the time-averaged streamwise velocity x/d = 25 downstream from the $\alpha = 45°$ pitched jet with C_μ^F=2.3, issuing into the boundary layer at the yaw angles $\beta = 0°$ (a), 30° (b), 60° (c), and 90° (d). The point of maximum momentum flux (defined as jet center) is marked using a white dot for reference.*

upwash underneath the jet. When the jet yaw increases to $\beta = 60°$ (Figure 3c), the spanwise position of its peak momentum migrates farther to the right and its elevation increases. It is noteworthy that the jet center moves closer to the CW vortex center (on the right) indicating spanwise imbalance in the distribution of jet momentum and deficit that is attributed to the blockage by the jet on its starboard side (right side, looking upstream). These data also show intensification and expansion of the in-plane flow associated with the CCW vortex while its center lies below the center of the CW vortex indicating that the latter may be advected around the former. Furthermore, while the CCW rotation increases, the peak momentum of the jet shifts toward the center of the CW vortex. These features are further intensified when $\beta = 90°$ (i.e., the jet issues in the spanwise direction, Figure 3d), as indicated by intensified left to right upwash and of the CCW flow accompanied by diminution of the streamwise velocity in the vicinity of its core, while the jet peak streamwise momentum is nearly centered on the somewhat weaker CW vortex. The variations of jet elevation above the surface and spanwise deflection relative to its orifice as measured by the y-z coordinates of its peak momentum in the y-z planes $x = 25d$, $50d$, and $75d$ is computed for each jet inclination $\alpha = 20°$, 32.5° and 45° over a range of yaw angles $0 < \beta < 90°$ ($C_\mu^F = 2.3$) and summarized in Figures 4a-c (the 7 yaw angles are increased in equal increments of 15° along each trace). These data show that while the elevation of the jet inclined at $\alpha = 20°$ generally increases (nearly monotonically) with β, the elevations of the higher pitch jets saturate or even reach a local maximum followed by a decrease. Close to the jet ($x/d = 25$, Figure 4a), the rates of increase in jet elevation with spanwise deflection are nearly the same for the three inclinations up to $\beta = 45°$. However, as β increases further, only the $\alpha = 20°$ jet continues to deflect away from the surface while the $\alpha = 32.5°$ and 45° jets reach a local peak and then their elevations diminish at the highest yaw angles ostensibly due to the increase in the speed of the cross flow with elevation within the boundary layer. The terminal elevation of the highest-inclination jet $\alpha =$ 45°, $y/\delta \approx 0.6$ (Figure 4b) is reached in the plane $x/d = 50$ and remains nearly unchanged at $x/d = 75$, Figure 4c), regardless of the yaw angle. However, the lower pitch jet $\alpha =$ 32.5° appears to be more sensitive to the yaw angle and its peak elevation diminishes for $\beta > 45°$ at $x/d = 50$ and 75 (Figures 4b and c). Nevertheless, it should be noted that unlike the $\alpha = 45°$ jet, the elevation of the $\alpha = 32.5°$ jet increases at all three measurement planes albeit at a lower rate than the $\alpha = 20°$ jet. It is remarkable that the spanwise deflection of the jets appears to be similar and nearly independent of their inclinations.

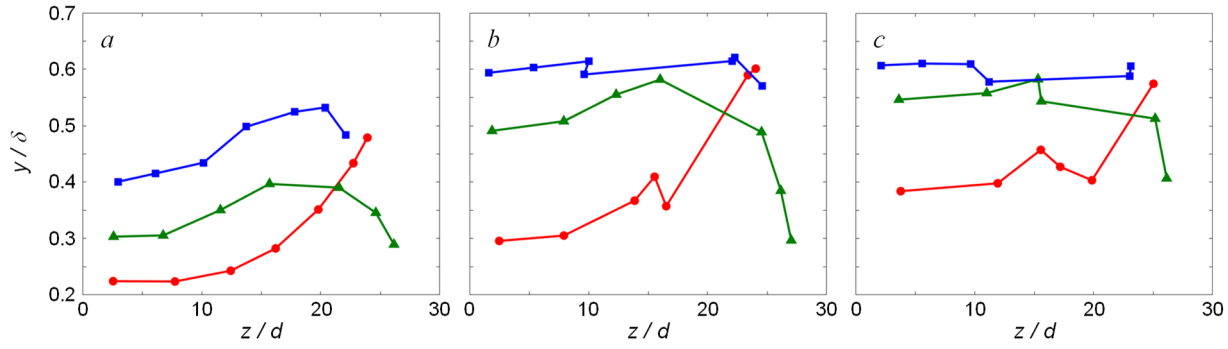

Figure 4. *Traces of the position of peak jet momentum ($C_\mu^F = 2.3$) in the y-z planes x/d = (a) 25, (b) 50, and (c) 75 for jet pitch $\alpha = 20°$ (●), 32.5° (▲), and 45° (■) and yaw angles $0° < \beta < 90°$ (increasing from left to right on each trace)*

The local attitude of each of the jets (issuing at $\alpha = 20°$, 32.5° and 45°) within the boundary layer is expressed in terms of the angular directions of its peak momentum vector or local pitch α' and yaw β' angles relative to each of the streamwise-normal planes (Figure 5). As shown in Figure 5a, the jet's local pitch α' for $\alpha = 20°$ increases with β and reaches a local maximum α' of about 23° at $\beta = 45°$ while the local pitch α' of the $\alpha = 32.5°$ and 45° appear to be saturated at about 25° below $\beta = 30°$ indicating the extent of their streamwise tilting upstream of the plane $x/d = 25$. The local pitch angles of the three jets diminish with increasing β and they become nearly identical but slightly positive as they align with the cross flow in Figure 5c (as expected, α' of each jet issuing at any yaw angle β diminishes monotonically with streamwise distance from the orifice). This pattern indicates that the jets become aligned with the cross flow within the boundary layer that is slightly diverging upward as the boundary layer expands into the cross flow. Figure 5d shows the variation of β' with the initial jet yaw. It is clear that the yawed jets turn rapidly in the streamwise direction and that the rate of this change increases with the pitch angle of the jet. For $\alpha = 20°$ the peak $\beta' \approx 15°$ at $\beta = 30°$ this is consistent with the largest spanwise deflection of the lowest inclination jet in Figure 4a. By $x/d = 75$, the yaw angle of all three jets nearly vanishes indicating virtually no effect of the orifice pitch angle on the local yaw. It is noteworthy that the local pitch angles of the three jets are nearly identical but still slightly positive, indicating slower relaxation of the pitch.

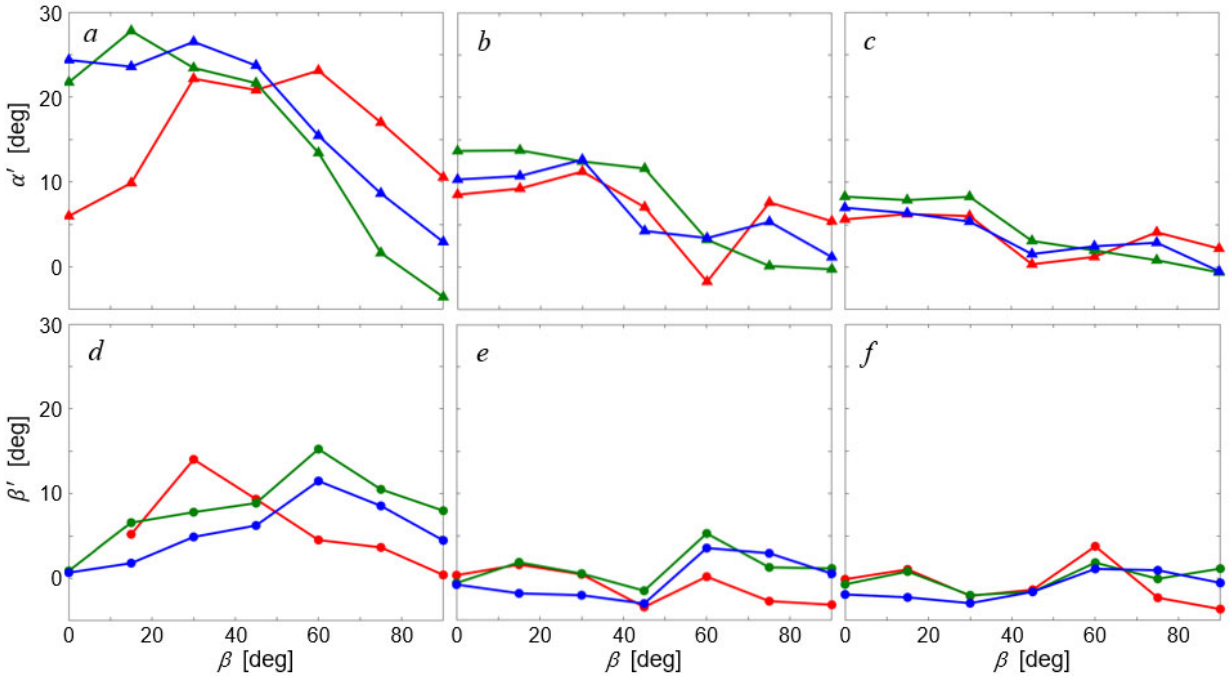

Figure 5. *Variation with β of the jet's pitch α′ (a-c, ▲) and yaw β′ (d-f, ●) angular attitude in the streamwise-normal planes x/d = 25 (a, d), 50 (b, e) , and 75 (c, f) for jet issuing at pitch angles α = 20°, 32.5°, and 45°.*

Considering the alignment of the jets relative to the cross flow by $x/d = 75$, the effect of each jet on the surrounding boundary layer flow is elucidated using an integral measure based on the increment of the cross-stream magnitude of streamwise flux of momentum per unit span at spanwise position z, $\Delta\varphi(z)$ relative to the base flow in the absence of the jet. Figures 6a-c show spanwise distributions of the normalized $\Delta\widehat{\varphi}(z) = \delta \cdot \Delta\varphi(z)/F$ (where δ is the boundary layer

thickness of the base flow and F is the magnitude of the jet force) for jets inclined at $\alpha = 20°$, 32.5°, and 45°, respectively ($C_\mu^F = 2.3$) at yawing angles $0 < \beta < 90°$. The distributions of $\Delta\widehat{\varphi}(z)$ for orifice yaw $\beta = 0$ show that at this streamwise location ($75d$ downstream of the jet orifice) the jet at $\alpha = 20°$ is reasonably symmetric about the peak flux ($z/d \approx 4$), the symmetry degrades somewhat with increasing α, (Figures 6b and c) ostensibly because of stronger interactions with the cross flow that are accompanied by pronounced spanwise spreading and significant reductions in the peak flux.

Furthermore, at $\alpha = 45°$, $\Delta\widehat{\varphi}(z)$ develops two peaks about the center of the jet that appear to be associated with the evolution of the jet's counter-rotating vortex pair (the peak at the CW (left) vortex is somewhat lower than at the CCW vortex (cf. Figure 3a). As the orifice yaw angle increases at $\alpha = 20°$ (Figure 6a), the distributions of $\Delta\widehat{\varphi}(z)$ become skewed as the jet spreads to the left owing to the yaw and its peak momentum diminishes monotonically. At $\beta < 90°$, the curve shifts to the left and there appears to be a momentum flux deficit (relative to the base flow) for $z/d > 30$. These trends are more accentuated at $\alpha = 32.5°$ and 45° (Figures 6b and c). At $\alpha = 32.5°$ the jet first exhibits a double peak at $\beta = 45°$ and, as noted above, the evolution at $\alpha = 45°$ already starts with a double peak at $\beta = 0$. Subsequently, both inclined jets ($\alpha = 32.5°$ and 45°) develop a strong momentum flux deficit over their starboard sides ostensibly as a result of low-speed fluid

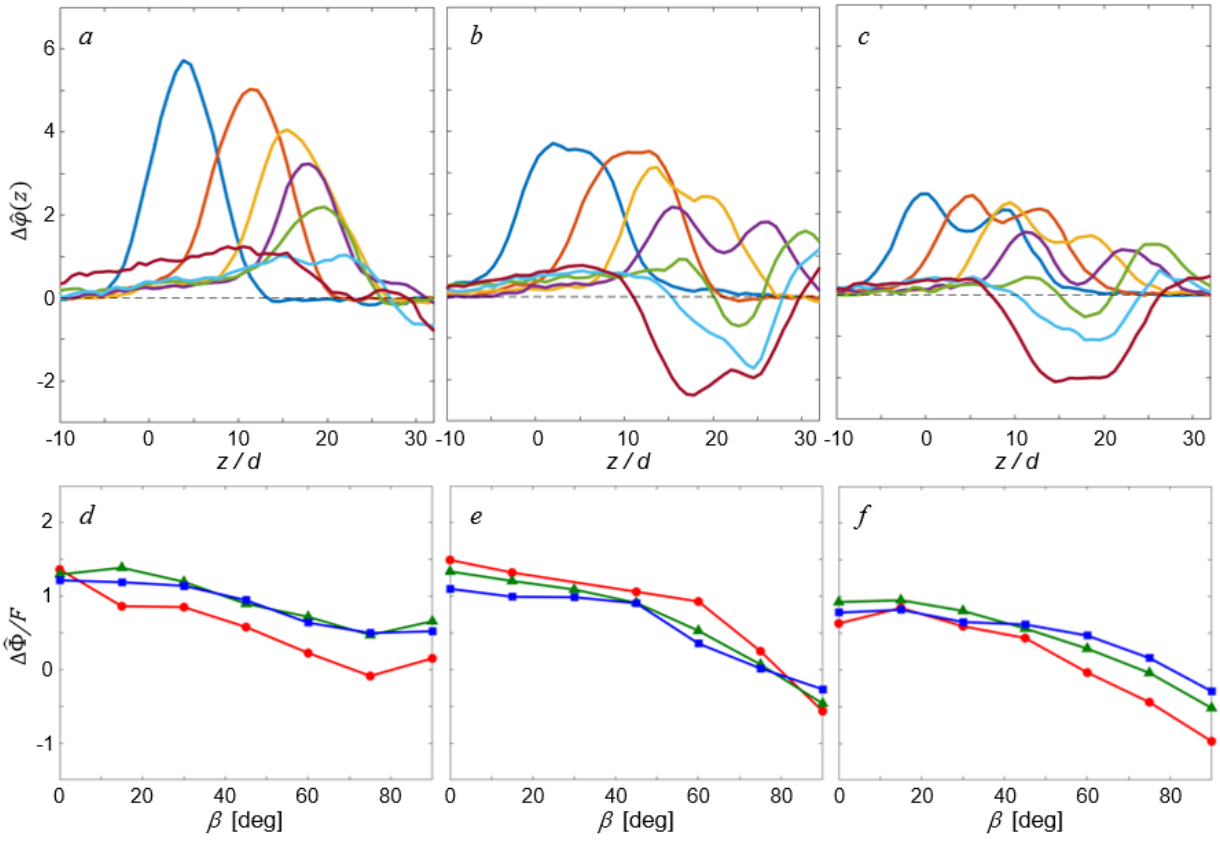

Figure 6. *a-c) Spanwise variation of the increment (relative to the base flow) of the normalized magnitude of streamwise flux of momentum per unit span $\Delta\widehat{\varphi}(z)$ at x/d = 75 for pitch angles $\alpha = 20°$ (a), 32.5° (b) , and 45° (c) and $\beta = 0°$ (—), 15° (—), 30° (—), 45° (—), 60° (—), 75° (—), and 90° (—); and d-e) Variation of spanwise-integrated $\Delta\widehat{\varphi}(z)$ at x/d = 75 $\Delta\widehat{\Phi}/F$ with orifice yaw angle and pitch angles $\alpha = 20°$ (d) , 32.5° (e), and 45° (f) for $C_\mu^F = 0.5$ (●), 2.3(▲), and 5(■).*

that is pulled up by the counter rotating vortex pair depicted in Figure 3. The data in Figures 6a-c show that aside from the inherent cross stream and spanwise spreading of transverse jets in cross flow, the imbalance between the counter rotating vortex pair (these effects are discussed further in connection with Figure 13). The effect of the jet on the momentum flux within the boundary layer is assessed by integration of the increment of streamwise flux of momentum $\Delta\varphi(z)$ across the span of the flow and the variation of the normalized spanwise-integrated flux increment $\Delta\widehat{\Phi}/F$ at $x/d = 75$ with orifice yaw angle is shown for three momentum coefficients ($C_{\mu}^{F} = 0.5$, 2.3, and 5) of each inclined jet $\alpha = 20°$, 32.5°, and 45° in Figures 6d-e, respectively. These data indicate that despite some scatter for a given jet inclination angle, $\Delta\widehat{\Phi}/F$ diminishes monotonically at this streamwise position with orifice β and nearly independently of the jet force F. It should be noted that for $\beta = 0$, $\Delta\widehat{\Phi} \approx F$ where variations may be attributed to interactions with the cross flow and the surface. Also, as noted in connection with Figures 6b and c, at high yaw and pitch angles the interactions of the jet with the flow lead to losses that are manifested by momentum deficit.

IV The Jet-Induced Vortical Structures

As discussed in §I, the interaction of a transverse jet with a cross flow results in the formation of a pair of counter-rotating vortices along the spanwise edges of the jet and the balance between their strengths or circulations varies with the jet's yaw angle. The effect of the orifice yaw angle on the formation and evolution of the counter rotating vortex pair is illustrated in color raster plots of time-averaged streamwise vorticity superposed with in plane velocity vectors in the streamwise-normal plane $x/d = 25$ of a jet inclined at $\alpha = 45°$ ($C_{\mu}^{F} = 5$). When the orifice $\beta = 0$ (Figure 7a) the interaction of the jet with the cross flow leads to the formation of a nearly symmetric vortex pair with pronounced induced upwash flow between them. However, when the jet issues at an orifice yaw of $\beta = 75°$ ($z > 0$, Figure 7b) the ensuing vortices are more complex since the CW (right) vortex is directly exposed to the oncoming cross flow while CCW vortex is 'shielded' on the opposite (leeward) side or wake of the jet flow. Consequently, these vortices evolve unevenly and the flow induced by the dominant CCW vortex along with the cross flow tends to rotate the weaker

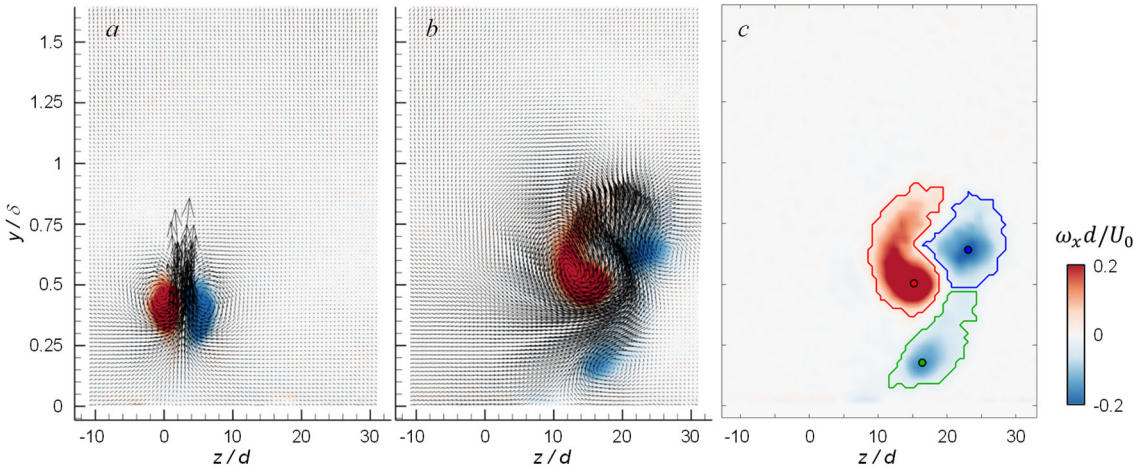

Figure 7. *Color raster plots of the time-averaged streamwise vorticity of a jet inclined at $\alpha = 45°$ ($C_{\mu}^{F} = 5$) in the streamwise-normal plane $x/d = 25$ at $\beta = 0°$ (a) and 75° (b). Using the Γ_1 criterion the vorticity data in (b) are replotted in (c) outlining the detected CCW (●) and CW (●) vortices along with the secondary CW vorticity (●) formed on the surface.*

CW vortex about the CCW vortex. When the dominant vortex circulation is sufficiently high it can spawn a secondary CW vortex off the surface as indicated by a secondary CW concentration. The evolution of these vorticity concentrations within the flow is assessed using the Γ_1 criterion (Graftieaux et al. 2001, Berson et al. 2009) to define the centers and bounds of vorticity concentrations. When applied to the flow field in Figure 7b, the resulting three vortical domains are depicted in Figure 7c and marked by red (CCW), blue (CW), and green (secondary CW vortex), along with their centers. It is noted that vortex 'centers' do not necessarily coincide with the local centers of rotation owing to residual shear of the jet, but as the effects of jet shear weaken farther downstream this offset in the vortex detection center diminishes.

The effect of the pitch and yaw angles of the jet orifice on the evolution and composition of the vorticity concentrations is shown in Figure 8 ($x/d = 25$ and $C_\mu^F = 2.3$) using color raster plots of the time-averaged streamwise vorticity where vorticity concentrations are again identified using the Γ_1 criterion, for jets inclined at $\alpha = 20°$, 32.5°, and 45°(columns *i-iii*) at orifice yaw $\beta = 0°$ - 90° (rows a-g). The symmetry of the vortex pair when $\beta = 0°$ is apparent in Figures 8a*i-iii* and the elevation of the vortices relative to the surface increases with pitch angle, reaching $y/\delta \approx 0.15$, 0.27, and 0.36°, respectively. At $\alpha = 20°$ as the yaw angle increases (Figure 8, column *i*) the CCW vortex intensifies and the CW weakens while the vortex pair is displaced (with the jet) in the spanwise direction and the weaker CW vortex rotates about the CCW vortex. As noted in connection with Figure 7c, the CCW vortex spawns a secondary CW vortex due to its interaction with the surface although at $\alpha = 20°$ these secondary vortices are rather weak. When α is increased to 32.5° (Figure 8 column *ii*), it appears that the higher penetration of the jet and vortex pair above the surface is associated with a lower spanwise displacement as β increases ostensibly owing to the lower resistance to cross flow underneath the jet and the change in relative elevations or induced rotation of the two vortices is less pronounced compared to $\alpha = 20°$. Simultaneously, the increased displacement from the surface leads to triggering secondary CW vortices at even lower yaw angles. Similar trends are observed at $\alpha = 45°$ (Figure 8 column *iii*) and it is noteworthy that the CW vortex becomes 'wrapped' by the dominant CCW vortex even if there is no clear rotation between their cores.

The CCW and CW vortices are characterized in Figure 9 by the vortex circulation Γ in the *x-z* plane (Figures 9a-c), and the increment in the induced normal volume flow rate ΔQ through the vortex relative to the base flow (figures 9d-f) for $C_\mu^F = 0.5$, 2.3, and 5. As shown in Figure 9a ($\alpha = 20°$) there is a significant disparity in the circulations of corresponding CCW and CW vortices for all levels of C_μ^F. While the circulation of the CCW increases monotonically with β and incrementally with C_μ^F, the circulation of the CW vortex reaches a local peak around $\beta \approx 60°$ and thereafter decays ostensibly through cancellation by the CCW vortex. In fact, at $C_\mu^F = 0.5$, the CW vortex is virtually completely diffused. Figure 9d shows that the corresponding maximum and minimum increments in volume flow rate relative to the base flow occur at $\beta \approx 60°$ and 0°, respectively, indicating that the presence of yaw leads to increased entrainment by the jet. Although there is generally a decrease in maximum vortex circulation with the increased jet inclination, Figures 9b and c show that the circulation of both the CCW and CW vortices at $\beta = 0$ increases with α, but its rate of increase with β is diminished and the CW circulation becomes nearly invariant with β regardless of C_μ^F. Also, there is some reduction in ΔQ through the vortex at high inclination angles (Figures 9e and f) and even a slight net deficit through the CCW vortex at

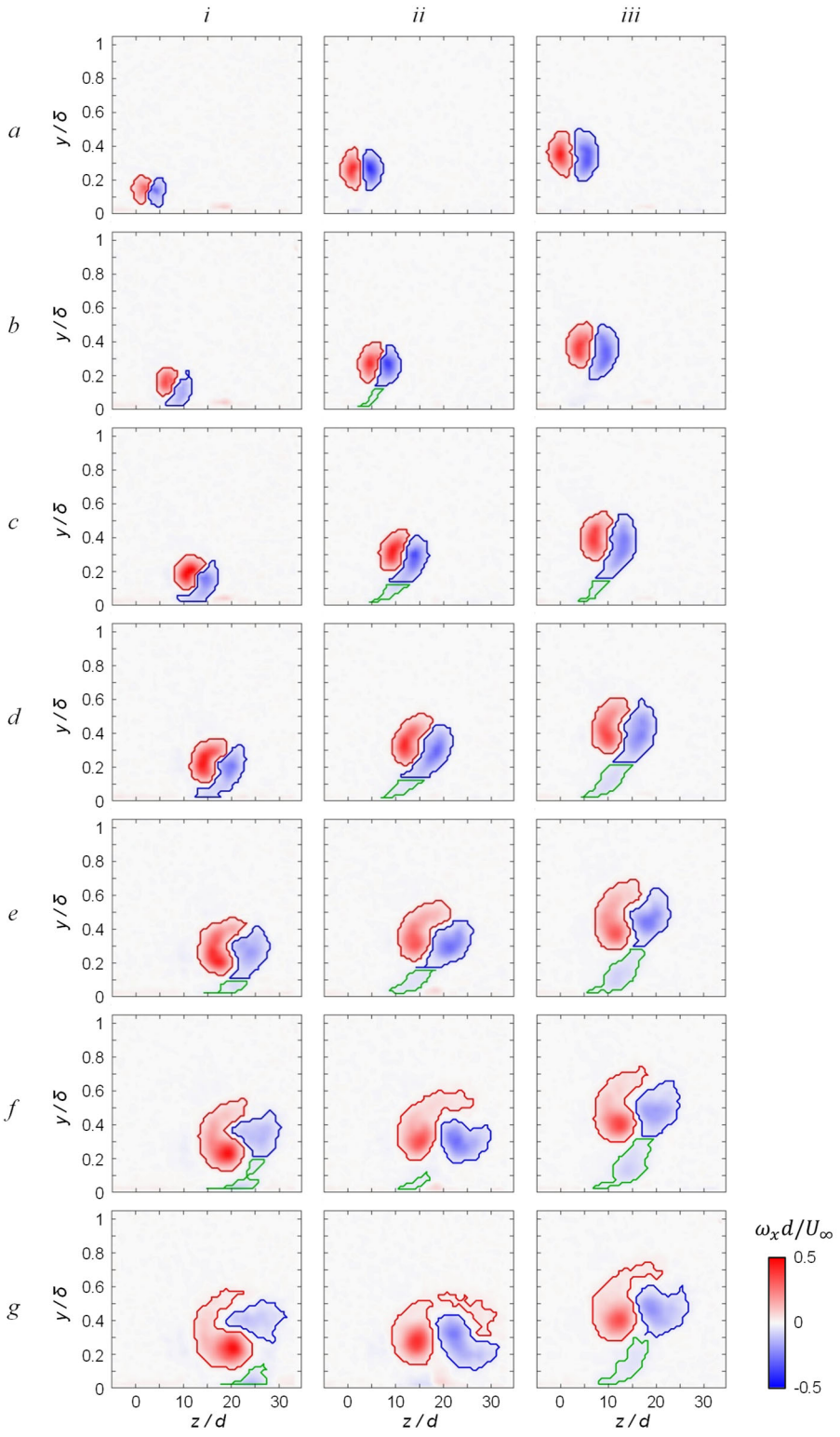

Figure 8. *Color raster plots of the time-averaged streamwise vorticity outlining using the Γ_1 criterion [CCW (●) and CW (●)] in the plane x/d = 25 for jets inclined at $\alpha = 20°$ 32.5° and 45° ($C_\mu^F = 2.3$) in columns i, ii, and iii, respectively, at orifice yaw $\beta = 0°$, 15°, 30°, 45°, 60°, 75°, and 90° (in rows a-g, respectively). When present, the secondary CW vorticity domain is marked (●).*

$C_\mu^F = 0.5$. The present data suggest that the circulation of the induced jet vortices and the increment in their internal flow rate increase with decreasing inclination.

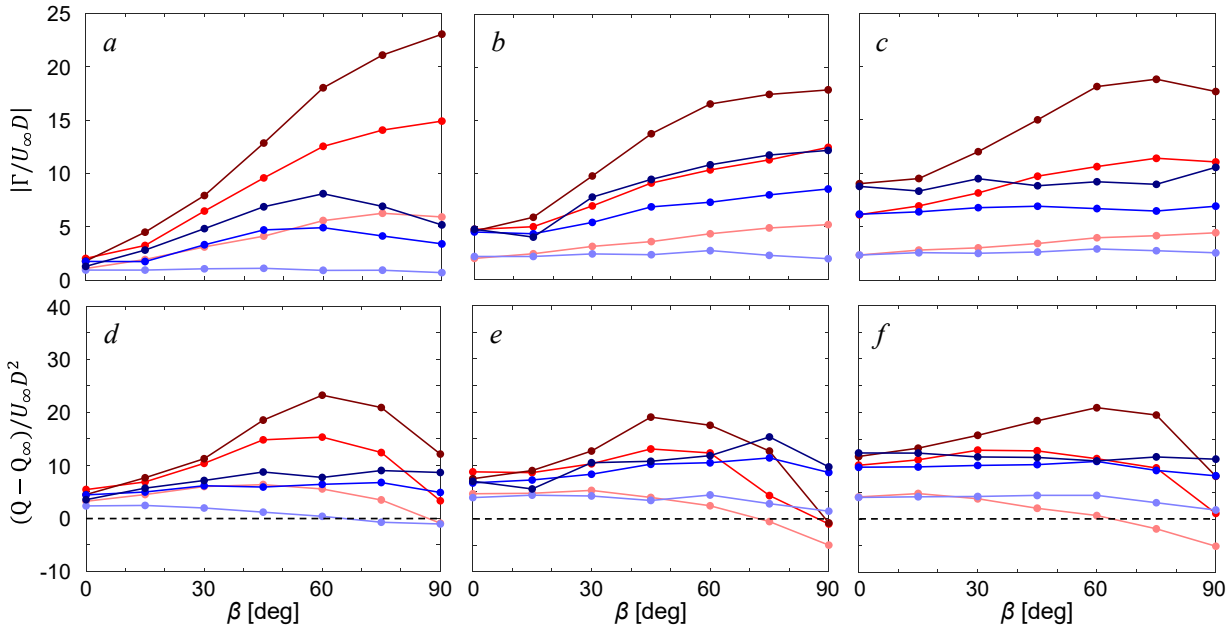

Figure 9. *Circulation (a-c) and volumetric flow rate gain (d-f) within the CCW (●) and CW (●) vorticity domains at x/d = 25 for α = 20° (a, d), 32.5° (b, e), and 45° (c, f) and C_μ^F= 0.5 (●,●), 2.3 (●,●), and 5 (●,●).*

V. Flow Interactions at $\alpha = 20^o$

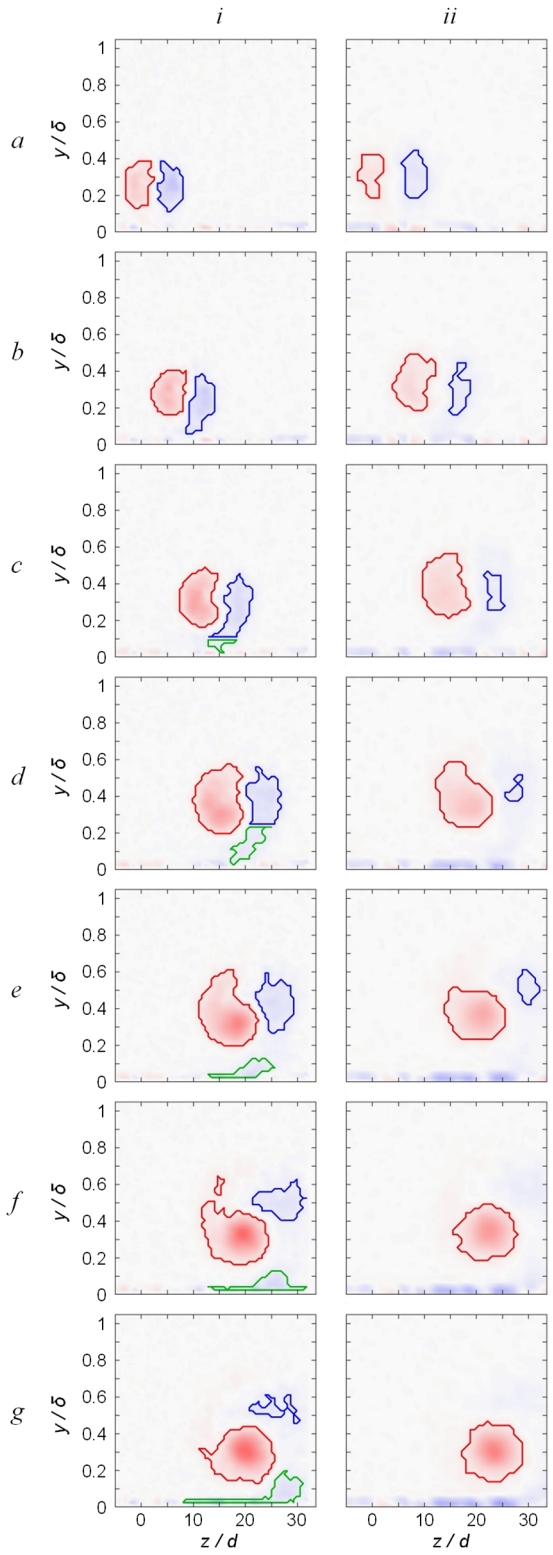

Figure 10. *As in Figure 8 for x/d = 50 (i) and 75 (ii).*

Based on the findings of §IV, in this section attention is restricted to the low-inclination jet at $\alpha = 20^o$. Continuing the discussion in connection with Figure 8 ($x/d = 25$) the evolution of the CCW and CW vorticity concentrations farther downstream from the orifice ($x/d = 50$ and 75) is depicted in Figures 10, columns *i* and *ii*, respectively. At $\beta = 0$, the elevation of the nearly symmetric vortex pair increases somewhat from $y/\delta = 0.15$ to 0.3 at $x/d = 25$ and 75, respectively, while the intensity of the vorticity concentrations diminishes. As β is increased the secondary CW vortex is detected at $x/d = 50$, but at $x/d = 75$ Figure 10 column *ii*, both the CCW and CW vortices appear to become isolated and weaker, and the remnants of the induced secondary concentrations are confined to the near-wall region. Furthermore, as β increases, the CW vortex weakens and ultimately vanishes (Figures 10ii-f and *ii*-g). *It is noteworthy that although it is commonly assumed that yawed jets would induce a single sense vortex whose sense depends on the yaw direction, the present investigations point to a rather resilient vortex pair, especially at high jet C_μ^F, and that a single vortex forms only after a prolonged coexistence of the vortex pair and after the dominant vortex becomes significantly weaker.*

Figure 11 shows the corresponding circulations and the increment of induced flow rate through the vortices relative to the base flow. It is noteworthy that at $\beta < 45°$, there is not much streamwise loss in circulation of the dominant CCW vortex (cf. Figures 9a and 11a and b), regardless of C_μ^F. The highest reduction in circulation of the CCW vortex occurs at higher yaw angles, most notably for $\beta = 75°$ and 90° indicating strong interactions with the surface and the CW vortex whose circulation is significantly lower. The corresponding evolution of the volumetric flow increment through the vortices, relative to the base flow, ΔQ exhibits several interesting trends. The flow rate carried by the CCW vortices is much higher than the CW vortex, except at the highest yaw angles when they

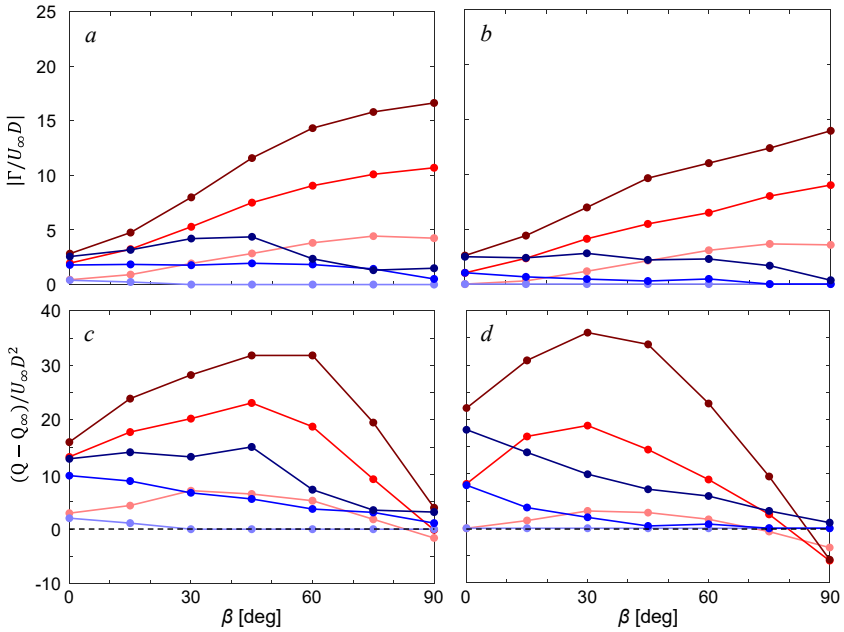

Figure 11. *As in Figure 9 for x/d = 50 (a, c) and 75 (b, d).*

become comparable. Also, as expected, the flow rate increment is proportional to C_μ^F and increases in the streamwise direction as an apparent consequence of the vortex entrainment. However, as discussed in section IV ($x/d = 25$), there is an optimum in the orifice yaw angle at which the flow transport through the vortices is maximized. These data indicate that while at for $x/d < 50$ (Figures 9a, 11c), this transport peaks at $\beta \approx 60°$ but shifts to $\beta \approx 30°$ at $x/d = 75$ (Figure 11d). The flow rate increment of the CW vortex exhibits a different trend. While its flow rate increment is less than half of that of the CCW vortex, it does not depend strongly on β. However, its flow rate increment increases downstream at low β, with the highest increment attained at $\beta = 0$ as is evident in Figure 11d.

As an indication of the vortex mixing, the turbulent kinetic energy TKE is estimated from the PIV measurements as $TKE = (\overline{u^2} + \overline{v^2} + \overline{w^2})/2$ and plotted in color raster plots within the vortices at $x/d = 25$ ($C_\mu^F = 2.3$) in Figures 12a–g. As expected, the strongest TKE signature is observed at the interaction interface between the two vortices (Figure 12a–d), where it initially intensifies with

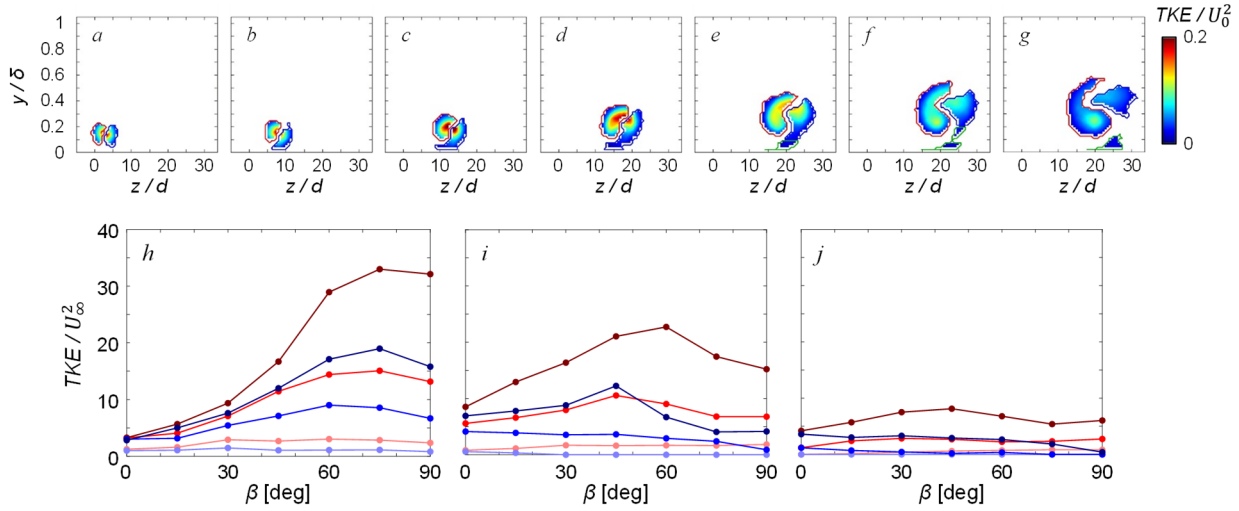

Figure 12. *a-g) Color raster plots of the time-averaged TKE at x/d = 25 for a jet inclined at α = 20° at C_μ^F = 2.3 at orifice yaw β = 0° (a), 15° (b) , 30° (c), 45° (d), 60° (e), 75° (f) , and 90° (g) within the detected CCW (●) and CW (●) vortical domains; and h-j) Cumulative TKE within the CCW (●) and CW (●) regions at x/d = 25 (h), 50 (i), and 75 (j) at C_μ^F = 0.5 (●,●), 2.3 (●,●), and 5 (●,●).*

increasing β, but past $\beta = 60°$, the domain of elevated TKE broadens while its peak magnitude diminishes. Also, as the CW vortex weakens at high β (Figure 12g), the broad TKE peak becomes associated with the CCW vortex flow. The variation with β of the cumulative TKE associated with each vortex at $x/d = 25$, 50, and 75 is shown in each of Figures 12h–j respectively for $C_\mu^F = 0.5$, 2.3, and 5. While the peak TKE levels clearly decrease at high β as shown in Figures 12a-g, the cumulative TKE associated with vortices clearly keeps increasing up to $\beta = 75°$ at $x/d = 25$ indicating that the broadening of the vortical domain with β overcomes the loss in intensity (the disparity between the TKE associated with CCW and CW vortices also increases with β). All the TKE levels notably drop at $x/d = 50$ (Figure 12i) as the jet spreads and continues to interact with the cross flow. It is also noted that the TKE associated with vortices at $C_\mu^F = 0.5$ is consistently low throughout at all three cross stream planes and depends only weakly on the yaw angle. At $x/d = 75$ (Figure 12j), all the TKE levels are significantly diminished indicating that the remnants of the jet and vortices are all but dissipated.

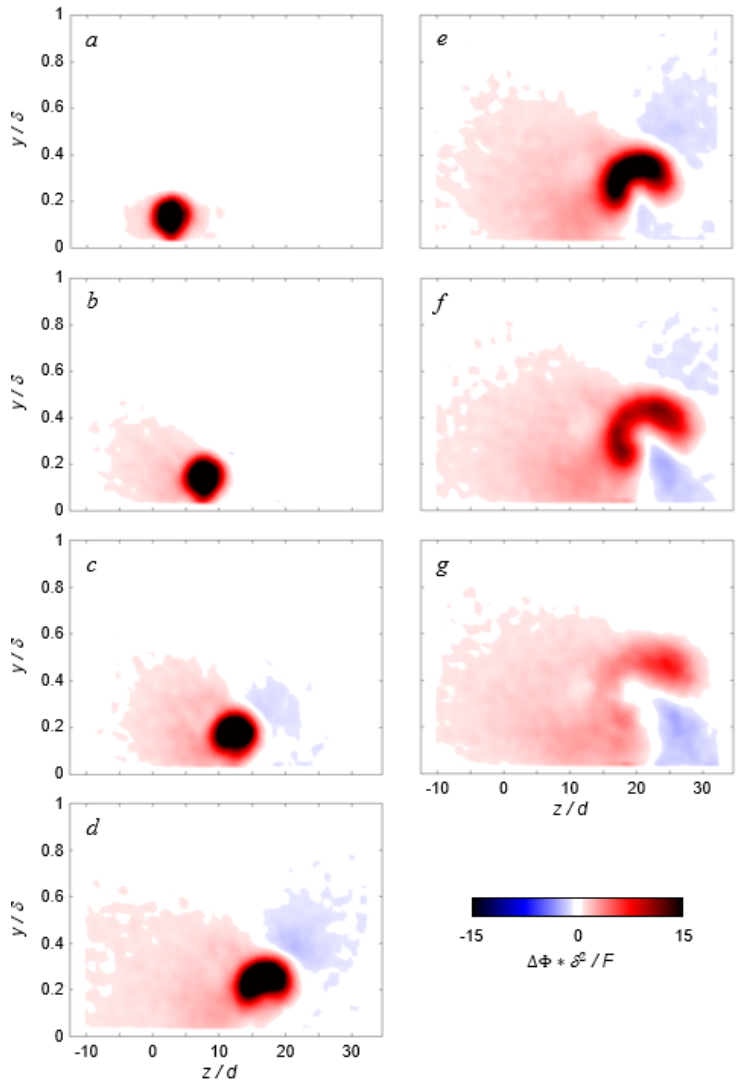

Figure 13. *Color raster plots of the time-averaged induced jet momentum flux gain x/d = 25 downstream from the $\alpha = 20°$ pitched jet with C_μ^F=2.3, issuing into the boundary layer at the yaw angles $\beta = 0°$ (a), 15° (b), 30° (c), 45° (d), 60° (e), 75° (f), and 90° (g).*

The impact of the jet on the surrounding boundary layer flow is assessed by the normalized increment of magnitude of the streamwise flux of momentum per unit area relative to the base flow $\Delta\Phi$. At $\beta < 30°$ (Figures 13a–c), the isolated domain of high momentum flux is concentrated about the jet and may be attributed to transport of higher momentum fluid by the (nearly symmetric) counter rotating vortices. At $\beta = 45°$ (Figure 13d) the induced CCW vortex is stronger and there is an apparent increase in the transport on the port side of the jet. As discussed in connection with Figure 3, the flow induced by the two vortices transports near-surface lower momentum fluid to the starboard side of the jet as manifested by the deficit at its top left. As the yaw is increased further (Figures 13e–g) and the CCW vortex intensifies, there is additional broadening of the domain of the increased momentum flux on the port side of the jet and momentum deficit on its starboard

side. For example, Figure 13g indicates an increase momentum flux across $-10 < z/d < 20$ and simultaneously, on the starboard side there is a smaller domain of momentum deficit within about $22 < z/d < 32$.

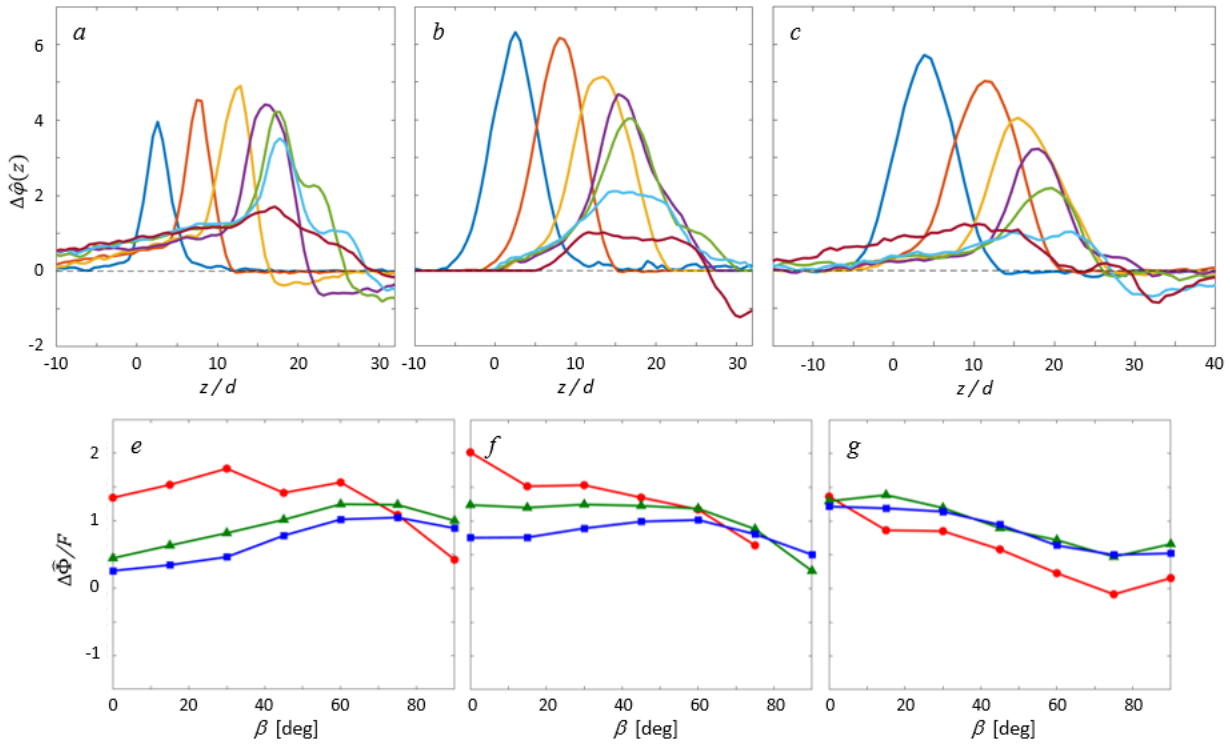

Figure 14. *a-c) Distribution of spanwise momentum increments ΔΦ (α = 20°) at x/d = 25 (a), 50 (b), and 75 (c) for β = 0° (—), 15° (—), 30° (—), 45° (—), 60° (—), 75° (—), and 90° (—); e -g) Variation of spanwise-integrated ΔΦ with yaw (α = 20°) at x/d = 25 (e), 50 (f), and 75 (g) for C_μ^F = 0.5 (●), 2.3(▲), and 5(■).*

Finally, similarly to Figures 6a–c, distributions of the momentum flux increment across the span across the planes $x/d = 25$, 50 and 75 for $C_\mu^F = 2.3$ are shown in Figures 14a–c. At $x/d = 25$ (Figure 14a), there is a consistent spanwise displacement of similar distributions of the momentum flux up to $\beta = 45°$, indicating a small but consistent loss of momentum flux on the starboard side of the jet. Past $\beta = 45°$, the spanwise distributions begin to broaden and flatten, owing to the increased losses due to the jet's increased blockage into the flow. For instance, the peak gain at $\beta = 90°$ is nearly four times lower than the peak gain at lower yaw. By $x/d = 50$ (Figure 14b), there is a significant increase in the magnitude of the flux (up to 50% increase in the peak increments at $\beta = 0°$ and 15°, although at $\beta = 0$ the jet exhibits some skewness), and at $x/d = 75$ (Figure 14c), the broadening of the spanwise effects continue, along with some reduction in peak magnitudes. The cumulative distributions of the normalized momentum flux increments at $x/d = 25$, 50 and 75 are shown in Figures 14e-g. These data show that the largest relative increment in the $x/d = 25$, 50, excluding the two highest yaw angles, are inversely proportional to C_μ^F, while showing some collapse of the distributions at $x/d = 50$ (Figure 14f). These results suggest that with the streamwise weakening of the direct jet effect, the prevailing vortex contributions to the momentum flux are at most weakly dependent on the jet momentum coefficient C_μ^F, and, combined with the prior analysis of Figures 6d-f, also weakly dependent on the jet pitch angle α.

VI. Conclusions

The present experimental investigation focuses on the interactions of a round surface jet with a nominally two-dimensional flat plate turbulent boundary layer [Re_x =O(10^6)] where the jet diameter is at least an order of magnitude smaller than the boundary layer characteristic thickness. Of specific interest is the effect of the jet's inclination (pitch) and yaw angles relative to the uniform flow above the boundary layer on spanwise distributions of cross stream momentum flux relative to the baseline boundary layer and the evolution of counter-rotating axial vortex pair that are induced by the shear between the cross flow and the jet and become uneven with increasing yaw angle. The jet is characterized using a modified momentum coefficient C_μ^F based on the ratio of the jet force F that is measured *in situ* and the momentum flux within the boundary layer over the jet orifice. The present investigation was conducted at three jet inclination angles (α = 20°, 32.5°, and 45°) , a range of yaw angles (0° < β < 90°), and three jet momentum coefficients (C_μ^F = 0.5, 2.3, and 5). The boundary layer over the inactive jet orifice was measured using planar PIV, in spanwise-normal planes and stereo PIV in three streamwise-normal planes (x/d = 25, 50, and 75) downstream of the jet orifice.

The effected spanwise momentum flux of the boundary layer flow in the presence of the jet develops domains of increased and decreased momentum relative to the base flow, and the extent of the momentum deficit increases with β. This drop-off in momentum flux becomes significant past β = 60° when the inclined jet develops a strong deficit over its starboard side that is accompanied by losses in total pressure.

The shear-induced counter rotating, nominally even axial vortex pair that forms on a streamwise jet in cross flow at zero yaw and becomes uneven when the jet is yawed relative to the cross flow. The axial vortex on the starboard side of the yawed jet becomes weaker with increasing yaw angle as the leeward side vortex intensifies. It is shown that the circulation of the axial vortices and spanwise distributions of the momentum flux increase with C_μ^F. The largest disparity between the vortex pair circulations was measured at the lowest pitch at which the dominant vortex had the highest circulation. Although it is commonly presumed that yawed jets in a cross flow induce a single sense vortex whose sense depends on the yaw direction, the present investigations show the formation of a rather resilient vortex pair, especially at high jet C_μ^F, and that a single vortex forms only after a prolonged coexistence of the vortex pair and after the dominant vortex becomes significantly weaker about 75d downstream of the jet orifice. Furthermore, the dominant vortex often spawns a secondary axial vortex off the surface such that, sufficiently far from the jet orifice, the flow includes three streamwise vortices, although the third vortex is delayed with decreasing pitch angle.

Acknowledgment/Disclaimer

This work was sponsored by the Office of Naval Research (ONR), under grant number N000142312500. The views and conclusions contained herein are those of the authors only and should not be interpreted as representing those of ONR, the U.S. Navy, or the U.S. Government.

References

Berson, A., Michard, M., and Blanc-Benon, P., "Vortex identification and tracking in unsteady flows," *Comptes Rendus Mécanique,* Vol. 337, No. 2, 2009, pp. 61-67.

Bray, T. P. and Garry, K. P. "Optimisation of Air-Jet Vortex Generators with Respect to System Design Parameters," *The Aeronautical Journal*, Vol. 103, No. 1028, 1999, pp. 475–479.

Compton, D. A., and Johnston. J. P., "Streamwise Vortex Production by Pitched and Skewed Jets in a Turbulent Boundary Layer," *AIAA Journal*, Vol. 30, No. 3, 1992, pp. 640-647.

Feng, Y-Y., Song, Y-P., and Breidenthal, R. E., "Model of the Trajectory of an Inclined Jet in Incompressible Crossflow," *AIAA Journal*, Vol. 56, No. 2, 2018, pp. 458-464.

Graftieaux, L., Michard, M., and Grosjean, N., "Combining PIV, POD and vortex identification algorithms for the study of unsteady turbulent swirling flows," *Measurement Science and Technology,* Vol. 12, No. 9, 2001, pp. 1422-1429.

Johnston, J., Nishi, M., Vortex generator jets — means for flow separation control, *AIAA Journal,* Vol. 28, 1990, pp. 989–994.

Johnston, J.P. "Pitched and Skewed Vortex Generator Jets for Control of Turbulent Boundary Layer Separation: A Review," Proceedings of the 3rd ASME/JSME Joint Fluids Engineering Conference, FEDSM99-6917, 1999.

Karagozian, A.R., "The Jet in Crossflow," *Physics of Fluids*, Vol. 26, No. 10, 2014, pp.1-47.

Mahesh, K., "The Interaction of Jets with Crossflow," *Annual Review of Fluid Mechanics*, Vol. 45, 2013, pp. 379-407.

Margason, R. J., "Fifty Years of Jet in Crosflow Research," In Computational and Experimental Assessment of Jets in Cross Flow, *AGARD-CP-534*, 1993.

Milanovic, I. and Zaman, K. B. M. Q. "Highly Inclined Jets in Cross Flow," *AIAA Paper 2003-183*, 2003.

Rixon, G. S. and Johari, H. "Development of a Steady Vortex Generator Jet in a Turbulent Boundary Layer," ASME. *J. Fluids Eng*., Vol. 125, No. 6, 2003, pp. 1006–1015.

Sharmishtha, C. and Utpal, B., "Review of Jets in a Cross Flow-Experimental and Numerical Approach," *International Journal of Engineering and Advanced Technology*, Vol. 7, No. 2, 2017, pp. 114-128.

Zhang, X. and Collins, M. W., "Measurements of a Longitudinal Vortex Generated by a Rectangular Jet in a Turbulent Boundary Layer," *Physics of Fluids*, Vol. 9, No. 6, 1997, pp. 1665-1673.